Tadros, M. A.; Farrell, K. E.; Schofield, P. R.; Brichta, A. M.; Graham, B. A.; Fuglevand, A. J. & Callister, R. J. "Intrinsic and synaptic homeostatic plasticity in motoneurons from mice with glycine receptor mutations" Published in the *Journal of Neurophysiology*, Vol. 111, Issue 7, (2014).

Available from: http://dx.doi.org/10.1152/jn.00728.2013

Intrinsic and synaptic homeostatic plasticity in motoneurons from mice with glycine receptor mutations

MA Tadros[1], KE Farrell[1], PR Schofield[2], AM Brichta[1], BA Graham[1], AJ Fuglevand[3] and RJ Callister[1]

[1]School of Biomedical Sciences & Pharmacy, Faculty of Health and Hunter Medical Research Institute, The University of Newcastle, Callaghan, NSW 2308, Australia
[2]Neuroscience Research Australia, Randwick, NSW 2031, Australia
[3]Department of Physiology, College of Medicine, University of Arizona, Tucson, AZ 85721-0093, USA

Running Title: motoneuron excitability in glycine receptor mutants

Key Words: action potential, GABA, excitability

Address for correspondence:
Dr. R.J. Callister
School of Biomedical Sciences & Pharmacy
The University of Newcastle
Callaghan, NSW 2308
Australia
Phone: Int-61-2-4921-7808
Fax:Int-61-2-4921-8712
Email: robert.callister@newcastle.edu.au

Abstract

Inhibitory synaptic inputs to hypoglossal motoneurons (HMs) are important for modulating excitability in brainstem circuits. Here we ask whether reduced inhibition, as occurs in three murine mutants with distinct naturally occurring mutations in the glycine receptor (GlyR), leads to intrinsic and/or synaptic homeostatic plasticity. Whole cell recordings were obtained from HMs in transverse brainstem slices from wild type (*wt*), spasmodic (*spd*), spastic (*spa*) and oscillator (*ot*) mice (C57Bl/6, ~ P21). Passive and action potential (AP) properties in *spd* and *ot* HMs were similar to *wt*. In contrast, *spa* HMs had lower input resistances, more depolarized resting membrane potentials, higher rheobase currents, smaller AP amplitudes and slower AHP current decay times. The excitability of HMs, assessed by "gain" in injected current/firing-frequency plots, was similar in all strains whereas the incidence of rebound spiking was increased in *spd*. The difference between recruitment and de-recruitment current (ie, delta-I) for AP discharge during ramp current injection was more negative in *spa* and *ot*. $GABA_A$ mIPSC amplitude was increased in *spa* and *ot* but not *spd,* suggesting diminished glycinergic drive leads to compensatory adjustments in the other major fast inhibitory synaptic transmitter system in these mutants. Overall, our data suggest long-term reduction in glycinergic drive to HMs results in changes in intrinsic and synaptic properties that are consistent with homeostatic plasticity in *spa* and *ot*, but not in *spd*. We propose such plasticity is an attempt to stabilize HM output, which succeeds in *spa* but fails in *ot*.

Introduction

Glycine receptors (GlyRs) mediate fast inhibitory synaptic transmission in the spinal cord and brainstem and are important for coordinating activity in motoneuron pools and subsequent skeletal muscle activation (Callister and Graham 2010; Legendre 2001; Lynch 2004). It is well known that acute reduction in GlyR-mediated inhibitory drive (eg, during strychnine poisoning) leads to increased motoneuron output in spinal cord and brainstem circuits and uncoordinated muscle activity in the form of convulsions or spasms (Owen and Sherrington 1911; Pratt and Jordan 1987). In contrast, longer-term manipulations that reduce inhibitory synaptic inputs in cultured neurons can result in altered intrinsic and synaptic properties in a manner that decreases neuron excitability and stabilizes circuit output (Turrigiano et al. 1998). Such "homeostatic plasticity" is now being increasingly examined, as it is clear that the effects of long-term alterations in synaptic drive on the output of neural circuits is important during development (Turrigiano and Nelson 2004) and in nervous system disorders (ElBasiouny et al. 2010; Mody 2005).

The murine mutants spasmodic (*spd*), spastic (*spa*) and oscillator (*ot*) have naturally occurring GlyR defects that result in long-term reductions to glycinergic drive. These mutants have contributed much to our understanding of the pentameric GlyR in cell lines, at native synapses, and at the in vivo or systems level of analysis (Graham et al. 2007b; Graham et al. 2006; Rajendra and Schofield 1995). All three mutants exhibit an exaggerated "startle response" when disturbed by loud noises or unexpected sensory stimuli (Simon 1995). In *spd,* a single point mutation in the α1 subunit of the GlyR results in reduced agonist sensitivity and single channel open time (Graham et al. 2011; Plested et al. 2007; Ryan et al. 1994). The *spa* mutation is caused by an intronic insertion of a LINE 1 transposable element in the β subunit gene, which causes exon-skipping and decreased transcriptional efficiency of β subunit protein (Kingsmore et al. 1994; Mülhardt et al. 1994). This results in markedly reduced GlyR expression assessed in spinal cord homogenates; however, channel properties are unaffected (Graham et al. 2003; Graham et al. 2006). The *ot* mouse has a microdeletion in exon 8 of the α1 subunit, which results in almost complete absence of α1 protein and functional GlyRs in the spinal cord and brainstem (Buckwalter et al. 1994; Kling et al. 1997). Thus, the *ot* mutation is considered a null mutation for the

88 adult (ie, α1/β) form of the GlyR. Within the first two to three weeks after birth the
89 three mutants exhibit a similar and easily recognized "startle" phenotype, which
90 suggests impaired control of motoneuron excitability (Biscoe and Duchen 1986;
91 Graham et al. 2006; Simon 1997).
92
93 In spite of these defects in inhibitory synaptic transmission two of the mutants, *spd*
94 and *spa*, survive and breed successfully. The *ot* mutant, however, dies about three
95 weeks after birth. Thus, these three mouse lines provide an opportunity to ask if long-
96 term impairment in glycinergic transmission can trigger changes in the intrinsic and
97 synaptic properties of motoneurons (ie, homeostatic plasticity), and whether this
98 differs between the mutants. We have examined this issue by studying a combination
99 of intrinsic and inhibitory synaptic properties in hypoglossal motoneurons (HMs)
100 from brainstem slices. We use HMs as our test neuron for several reasons. HMs
101 innervate muscles of the tongue and their excitability plays a critical role in
102 behaviours such as chewing, swallowing, suckling, vocalization and respiration
103 (Berger et al. 1995; Lowe 1980). In addition, their output is strongly modulated by
104 glycinergic inhibitory synaptic transmission (Cifra et al. 2009; Singer et al. 1998;
105 Umemiya and Berger 1995) and HMs appear to be one of the few motoneuron
106 populations that can be studied in both juvenile and adult animals (Callister et al.
107 1999; Graham et al. 2006).
108

Materials and Methods

Animals

Experiments were undertaken on wild type (*wt*), spasmodic (*spd*), spastic (*spa*) or oscillator (*ot*) mice (both sexes) backcrossed onto the C57Bl/6 background. The University of Newcastle Animal Care and Ethics Committee approved all procedures. The mutant lines were originally obtained from the Jackson Laboratory (Bar Harbor, ME). Most mutant animals and all *wt* controls were bred at the University of Newcastle. Some additional *spd* animals were obtained from an identical line bred at Australian BioResources (Moss Vale, NSW, Australia). *Spd*, *spa,* and *ot* mice were bred by mating heterozygous (*spd*/+, *spa*/+ and *ot*/+) animals, resulting in 25% of the progeny being homozygous. Animals were maintained on a 12:12 hr light:dark cycle and given unlimited access to food and water. Homozygous affected animals exhibited the exaggerated "startle" response and were easily identified ~ 2 weeks after birth according to four criteria: (1) limb clenching when picked up by the tail, (2) an impaired righting reflex, (3) a constant tremor at rest, and (4) walking on tiptoe with an arched back (Graham et al. 2006; Simon 1997).

Tissue Preparation

Mice were anaesthetised with ketamine (100 mg/kg i.p.) and decapitated. The brainstem was rapidly removed and immersed in ice-cold sucrose-substituted artificial cerebrospinal fluid (sACSF) containing (in mM): 250 sucrose, 25 $NaCHO_2$, 10 glucose, 2.5 KCl, 1 NaH_2PO_4, 1 $MgCl_2$ and 2.5 $CaCl_2$, continuously bubbled with 95% O_2 and 5% CO_2. The brainstem was placed on a Styrofoam support block and glued rostral side down onto a cutting stage with cyanoacrylate glue (Loctite 454; Loctite, Caringbah, Australia). The cutting stage was placed into a cutting chamber containing ice-cold, oxygenated sACSF. Transverse slices (300 µm thick) were obtained from the region of the brainstem containing the hypoglossal nucleus (~ 0.5 mm above and below the obex) using a vibrating-blade microtome (Leica VT1200s, Leica Microsystems, Wetzlar, Germany). The three to four slices containing the hypoglossal nucleus were transferred to a humidified storage chamber containing oxygenated ACSF (118 mM NaCl substituted for sucrose in sACSF). Slices were

allowed to recover for 1 hour at room temperature (22 - 24°C) before recording commenced.

Electrophysiology

Brainstem slices were transferred to a recording chamber, and held in place using nylon netting fixed to a U shaped platinum frame. The recording chamber was continually super-fused with oxygenated ACSF (4 - 6 bath volumes/minute) and maintained at a constant temperature (23°C) using an in-line temperature-control device (TC-324B, Warner Instruments, Hamden, CT). Whole cell patch clamp recordings were obtained from hypoglossal motoneurons (HMs), visualized using infrared differential contrast optics (IR-DIC optics) and an IR-sensitive camera (Rolera-XR, Olympus, NJ). HMs were easily identified according to their large soma size (diameter 20-35 µm vs. 10-15 µm for local interneurons), high capacitance (>35 pF), and low input resistance (70 - 80 MΩ) (Graham et al. 2006).

Intrinsic properties of HMs

Patch pipettes (3-4 MΩ resistance) were prepared from thin walled borosilicate glass (PG150T-15, Harvard Apparatus, Kent, UK), and filled with a potassium-based internal containing (in mM): 135 KCH_3SO_4, 6 NaCl, 2 $MgCl_2$, 10 HEPES, 0.1 EGTA, 2 MgATP, 0.3 NaGTP, pH 7.3 (with KOH). Whole cell patch clamp recordings were made using a Multiclamp 700B Amplifier (Molecular Devices, Sunnyvale, CA). The whole cell recording configuration was first established in voltage clamp mode (holding potential - 60 mV). Series resistance was measured from the averaged response (five trials) to a 5 mV hyperpolarizing pulse. This was measured at the beginning and end of each recording session and data were rejected if values changed by > 20%. Input resistance was obtained by calculating the chord conductance across a minimum of four responses to incrementally increasing hyperpolarizing current injections (50 pA increments in current clamp recording mode).

Once the whole cell recording mode was established, several stimulus protocols were applied to each HM to study intrinsic properties. Firstly, in voltage clamp, we assessed the characteristics of the AP afterhyperpolarisation (AHP) current. This was recorded at -60 mV following the delivery of a 2 ms pulse to -10mV. This pulse was

174 delivered every 4 s (10 times) and the responses were averaged for analysis. We then
175 switched the recording mode to current clamp and the membrane potential recorded ~
176 15 s after this switch was taken as the neuron's resting membrane potential (RMP).
177 All membrane potential values have been corrected for a calculated 10 mV liquid
178 junction potential (Barry and Lynch 1991). In order to record single APs a series of
179 short duration depolarising steps (20 pA increments, 2 ms duration) were applied
180 from RMP. Several measurements were then made on these APs (see Table 2). Small
181 bias currents (< 50 pA) were then injected into the recorded HM to maintain
182 membrane potential at -70 mV. AP discharge was examined from this potential by
183 applying: 1) a series of long depolarising and hyperpolarizing current steps (50 pA
184 increments, 1 s duration); and 2) triangular ramp currents (peak amplitude of 1 nA,
185 3.5 s rise and fall). Rheobase current was taken as the minimum current needed to
186 evoke an AP during a 1 s period of depolarizing current injection.
187
188 *Properties of GABAergic quantal currents (mIPSCs) in HMs*
189 We have shown previously in spinal cord dorsal horn neurons that reduced
190 glycinergic drive in *spa* is accompanied by compensatory upregulation in
191 $GABA_A$ergic neurotransmission (Graham *et al.,* 2003). Therefore, in a separate series
192 of experiments we recorded $GABA_A$-mediated miniature inhibitory postsynaptic
193 currents (mIPSCs) from HMs in each genotype. All experiments used patch pipettes
194 filled with a caesium chloride-based internal solution containing in mM: 140 CsCl, 10
195 HEPES, 10 EGTA, 2 ATP, and 0.3 GTP (pH adjusted to 7.3 with 1M CsOH, 21-23
196 ºC). Holding potential was set at -70 mV and $GABA_A$ergic mIPSCs were
197 pharmacologically isolated by application of CNQX (10 µM), strychnine (1 µ) and
198 TTX (1 µ) to the bath solution. Drugs were applied to the slice for a minimum of 3
199 minutes before data capture commenced. $GABA_A$ergic currents were recorded for 4-6
200 minutes. Application of bicuculline (10 µM) blocked all synaptic activity, indicating
201 that the mIPSCs recorded were mediated via activation of $GABA_A$ receptors (n = 3
202 for each genotype).
203
204 ***Data capture and analysis***
205 *Intrinsic properties of HMs*

206 Data were digitised on-line (sampled at 20 kHz, filtered at 6 kHz) via an ITC-16
207 computer interface (Instrutech, Long Island, NY) and stored on a Macintosh computer
208 using Axograph X software (Molecular Devices, Sunnyvale, CA). All data were
209 analysed offline using the Axograph software. The AHP current recorded in voltage
210 clamp was averaged (10 trials), and the amplitude and latency of the maximum
211 outward current after the large inward current (or action current) were measured
212 (Callister et al. 1997). An exponential was fit to the decay phase of the response in
213 order to calculate the AHP current decay time constant.
214
215 Onsets of APs were identified using the derivative-threshold method to detect the
216 inflection point; with dV/dt set at 20 mV/ms. AP properties were measured for
217 rheobase APs, generated by short duration depolarising steps (20 pA increments, 2 ms
218 duration). The rheobase current was taken as the minimum current step that would
219 evoke one AP. The difference between AP threshold and the maximum positive peak
220 was taken as AP amplitude. AHP current amplitude was measured as the difference
221 between AP threshold and the maximum negative peak. Finally, AP half-width was
222 measured at 50% of the AP's maximum positive peak.
223
224 The derivative threshold method was also used to detect APs evoked during injection
225 of long duration depolarising steps and slow triangular current ramps. We calculated
226 the instantaneous frequency as the reciprocal of the interspike interval. Mean AP
227 frequency was taken as the average of all instantaneous frequencies for APs evoked
228 by a single current step. Frequency/current plots (F/I plots) were generated using
229 mean frequency (per current step) and the corresponding current amplitude.
230
231 For the APs discharged during triangular current injection trials, instantaneous AP
232 frequency was calculated as above and the currents associated with onset (recruitment
233 current) and cessation of spiking (de-recruitment current) were measured. The
234 difference between these two values (ie, de-recruitment current minus recruitment
235 current), referred to as ΔI (Bennett et al. 2001b) was calculated. Positive ΔI values
236 occur when neurons stop firing at injected current values larger than that at which
237 they were recruited and are consistent with a dominant role of active conductances
238 underlying firing rate adaptation. Negative ΔI values, on the other hand, occur when

239 the injected current associated with de-recruitment is less than the amount needed for
240 recruitment. This likely indicates activation of persistent inward currents (Bennett et
241 al. 2001b; Button et al. 2006; Pambo-Pambo et al. 2009; Turkin et al. 2010).
242
243 *Propeties of GABAergic mIPSCs in HMs*
244 GABAergic mIPSCs were filtered at 2 kHz, recorded onto videotape (A.R. Vetter Co.,
245 Rebersberg, PA, USA), and either simultaneously or subsequently digitised (sampled
246 at 10 kHz) using WCP software (kindly provided by J. Dempster, Strathclyde
247 Electrophysiology Software, Glasgow, UK). This software enabled the detection and
248 analysis of mIPSC properties for each recorded cell. The detection threshold for
249 synaptic events was set just above background noise levels (~ 5 pA). A plot of mIPSC
250 amplitude vs. record number was constructed to ensure there were no changes (ie,
251 rundown) in recording conditions during each experiment. If an obvious trend in
252 mIPSC amplitude was detected, data were rejected. Mean values for mIPSC rise-time
253 (calculated over 10 - 90% of peak amplitude), peak amplitude, and decay time
254 constant (calculated over 20 - 80% of the decay phase) were obtained for each cell
255 using automated procedures within the WCP program. Mean mIPSC frequency was
256 obtained by dividing the number of captured events by the recording time in seconds.
257
258 ***Statistics***
259 All analysis was undertaken using SPSS software (SPSS v.10, SPSS Inc, Chicago,
260 IL). ANOVA was used to compare variables across genotypes. Scheffe post hoc tests
261 were used to determine which genotypes differed. Data that failed Levene's test for
262 homogeneity of variance were compared using the nonparametric Kruskal-Wallis test,
263 followed by Tamhane's T2 post hoc test. G-tests, with Williams' correction, were
264 used to determine if the incidence of rebound spiking differed between genotypes.
265 Statistical significance was set at $P < 0.05$ and all data are presented as means ± SEM.
266
267 ***Drugs***
268 TTX was obtained from Alomone Laboratories (Jerusalem, Israel). CNQX and
269 strychnine were purchased from Sigma (St. Louis, MO, USA).
270
271

272 **Results**

273 Figure 1 and Table 1 summarize the effect of each glycine receptor mutation on
274 glycinergic mIPSCs in HMs. The data for homozygote mutant animals have been
275 reported previously (Graham et al., 2006). Here we compare these data from the
276 different mutant genotypes to wildtype HMs, rather than between hetero- and
277 homozygotes, as our previous paper. Each mutation dramatically reduced glycinergic
278 mIPSC amplitude compared to *wt* values in the order *spd* > *spa* > *ot* (Fig 1 and Table
279 1). This was most notable in the *spa* and *ot* mutants. The effect of each mutation on
280 GlyR kinetics varied: mIPSC decay time was unaltered in *spa*, decreased in *spd*, and
281 increased in *ot* (Table 1). Together, these data show the three mutations dramatically
282 effect GlyR-mediated inhibition, but via different physiological mechanisms.

283

284 The presence of any GlyR mediated mIPSCs in the *ot* animals is worthy of comment
285 as this mouse is considered a null mutation for the adult form of the GlyR
286 (Buckwalter et al. 1994; Kling et al. 1997). In Graham et al., 2006 we suggested the
287 few mIPSCs we recorded in *ot* HMs were generated by fetal glycine receptors (ie,
288 containing α2 subunits), which persist after the switch from the fetal to adult form of
289 the GlyR at about P14. This interpretation is supported by the slower decay time of
290 GlyR mIPSCs in the *ot* animals (Table 1), a distinguishing feature of fetal GlyRs
291 (Singer et al 1998). We believe the best explanation for the low mIPSC frequency is
292 that there are only a few GlyR clusters (ie, synapses) in *ot* HMs.

293

294 ***Intrinsic properties of HMs***

295 Data on the intrinsic properties of HMs were obtained from 230 HMs from 57 animals
296 (*wt* = 16; *spd* = 17; *spa* = 12; and *ot* = 12). Data were grouped according to genotype
297 and the mean age (days) for each genotype is presented in Table 2. We made every
298 effort to ensure animals were age-matched at the time of recording, however, the
299 mean age of *spd* and *ot* animals differed from wt. *Spd* animals were slightly older
300 (25.2 ± 0.8 vs 21.3 ± 0.5 days). *Ot* animals were younger (18.6 ± 0.1 vs 21.3 ± 0.5
301 days) because the oscillator mutation is lethal by ~P21. Previous studies on the
302 development of inhibitory synaptic transmission in HMs suggest such comparisons
303 are valid (Singer et al. 1998).

304

305 ***Membrane and action potential properties***

306 Results for membrane and action potential properties of HMs across genotypes are
307 shown in Table 2. Input resistance (R_{IN}) and resting membrane potential (RMP) were
308 similar in *wt*, *spd* and *ot* HMs. In contrast, *spa* HMs had lower input resistance and a
309 more depolarised RMP compared to both *wt* data and the other mutants. Furthermore,
310 AP threshold was more depolarised in *spa* and *ot* HMs compared to *wt*. As might be
311 expected, based on their lower input resistance and higher AP threshold, rheobase
312 current was higher in *spa* HMs. In addition, *spa* HMs had smaller AP amplitudes
313 compared to *wt* HMs. Collectively, these results indicate *spa* HMs exhibit a reduced
314 intrinsic excitability.

315

316 ***Properties of action potential afterhyperpolarisation***

317 We recorded the outward afterhyperpolarisation (AHP) current in HMs by injecting a
318 large depolarising pulse (to -10 mV from a holding potential of -60 mV, 2 ms
319 duration) and compared the properties of the AHP current across genotypes (Fig. 2).
320 No significant differences were observed in the amplitude of the AHP current (Fig.
321 2B), however, the decay time constant of the AHP current was longer in *spa* HMs
322 compared to *wt* (Fig. 2C), suggesting that potassium conductances underlying the
323 AHP current are prolonged in this mutant.

324

325 ***Responses to depolarizing current injection***

326 Injection of square current steps of increasing amplitude (50 pA increments, from a
327 membrane potential of -70 mV, 1 second duration) resulted in tonic AP discharge in
328 HMs from all four genotypes. Example responses to three levels of current injection
329 in a *wt* HM are shown in Figure 3A with plots of the associated instantaneous
330 frequency during the current steps shown in Figure 3B. As shown previously for
331 spinal MNs in cats and mature HM in rats (Kernell 1965; Sawczuk et al. 1995; Viana
332 et al. 1995), firing frequency declined markedly during the current step and the
333 magnitude of the decline was greater for larger current steps. Such spike-frequency
334 adaptation was a feature of all HMs examined from all genotypes.

335

336 To characterize the steady state F/I relationship for each neuron, mean frequency was
337 measured for each level of injected current. To facilitate averaging among neurons
338 within a genotype, current values were normalized to each neuron's rheobase current.

339 Such normalized F/I data indicate the change in discharge frequency with increased
340 current (in pA) above rheobase. Figure 3C shows the averaged F/I relation for each
341 genotype with each curve offset along the horizontal axis by the average value of the
342 rheobase current for that genotype. From these F/I relationships, we compared three
343 features that represent different aspects of intrinsic excitability across genotypes: 1)
344 rheobase current indicating how readily a neuron can be brought to threshold for
345 *repetitive* discharge, 2) discharge frequency at rheobase indicating the minimal
346 frequency upon which discharge rate can be modulated, and 3) gain (average slope of
347 F/I relation) indicating the efficacy by which increases in depolarizing current are
348 transformed into augmented spike-frequency output. A fourth feature, namely
349 maximal firing frequency, was not measured because we did not deliver the high
350 levels of current required to reach depolarization blockade of APs, associated with
351 maximal firing rates (eg, (Pilarski et al. 2011). Of the above features only rheobase
352 current differed: specifically it was increased in *spa* (Table 2). Thus, *spa* HMs appear
353 less susceptible to being brought to spiking threshold, however, once activated HMs
354 in all strains respond similarly to depolarizing current modulation.
355
356 ***Responses to hyperpolarizing current injection***
357 We next examined the response of HMs to hyperpolarizing current injection as this is
358 often examined in motoneurons to assess the properties of the hyperpolarization-
359 activated mixed cationic inward current (I_h). This current is highly expressed in adult
360 HMs (Bayliss et al. 1994) and spinal MNs (Takahashi 1990) and plays a role in
361 regulating AP discharge by modulating the amplitude and time course of synaptic
362 inputs (Reyes 2001). The response of HMs to hyperpolarisation was assessed via
363 injection of hyperpolarising current steps (-50 pA increments, 1 s duration) until peak
364 membrane hyperpolarization reached -110 mV. Depolarizing 'sag' was used as an
365 index of I_h magnitude and was quantified as the ratio of the peak hyperpolarized
366 membrane potential at the outset of the hyperpolarizing current pulse to that at the
367 termination of the pulse (Fig. 4A solid and open arrowheads). Sag ratios did not differ
368 across the four genotypes, however, more current was required to hyperpolarize *spa*
369 HMs to -110 mV compared to *wt* (-664 pA ± 22 vs 594 ± 15 pA), consistent with their
370 lower input resistance (Table 2).
371

372 Upon removal of the hyperpolarizing pulses, all HMs exhibited some degree of
373 rebound depolarization. This was of sufficient magnitude in some neurons to elicit
374 spiking (Fig. 4A left panel). The proportion of neurons exhibiting rebound spiking
375 was greater in *spd* compared to *wt* animals (Fig. 4B). These data suggest there is a
376 selective change in the currents activated by the release from hyperpolarization in *spd*
377 HMs.
378
379 ***Responses to triangular current ramps***
380 We also measured the response to triangular ramp current injections (1 nA peak with
381 3.5 second rise and fall; holding potential -70 mV) as this procedure has been used to
382 investigate and test for engagement of active conductances in motoneurons (Bennett
383 et al. 2001b; ElBasiouny et al. 2010; Theiss et al. 2007) and dorsal horn neurons
384 (Reali et al. 2011). Figure 5A shows an example response in a *wt* HM to triangular
385 current injection and Figure 5B shows the associated F/I plot for the rising and falling
386 phases of the current injection. As outlined in the Methods, ΔI (current at cessation of
387 spiking minus current at onset of spiking) was calculated for each neuron to provide
388 an indirect assessment of the influence of two competing forms of active
389 conductances - those related to spike-frequency adaptation (giving rise to positive ΔI
390 values) and those associated with persistent inward currents (PICs; which yield
391 negative ΔI values).
392
393 Figures 5C-F show histograms of ΔI values obtained for each of the four strains.
394 Mean ΔI values (Fig. 5G, Table 2) were all near zero pA although slightly positive for
395 *wt* and modestly negative for *ot*. A Kruskal-Wallis test indicated a significant effect of
396 genotype on ΔI; and post-hoc testing indicated a significant difference in ΔI values
397 between *wt* and both *spa* and *ot*. When normalized to rheobase current, the average ΔI
398 represents, for example, ~0.08 × rheobase for *ot* mutants. This implies that PICs
399 provided only about 8% of the current needed to recruit and sustain *in vitro* activity in
400 HMs in the *ot* mouse. This stands in contrast to the highly enhanced PICs (~50% of
401 rheobase) observed in sacral MNs of adult rats following chronic spinal cord injury
402 (Bennett et al 2001a). As such, there appears to be relatively modest adaptations in the
403 active conductances underlying firing rate adaptation ***or*** PICs as a consequence of
404 GlyR mutations and these are confined to the *spa* and *ot* mutants.

405

406 ***Properties of GABAergic mIPSCs***

407 GABAergic mIPSC propeties were investigated in a separate series of experiments
408 because intrinsic properties and inhibitory synaptic currents cannot be studied with
409 the same internal pipette solution. mIPSC data were obtained from 58 HMs from 21
410 animals (*wt* = 7; *spd* = 5; *spa* = 5; and *ot* = 4). As in our experiments on intrinsic
411 membrane properties every effort was made to age match animals, however, *spd*
412 animals were slightly older than *wt* animals (27.3 ± 0.7 vs 20.0 ± 0.2 days).

413

414 The properties of GABAergic mIPSCs in the four strains are summarized in Table 3
415 and Figure 6. The rise and decay times were similar for mIPSCs in all strains (~ 2.0
416 and 15 ms, respectively, Table 3). Although mIPSC frequency varied considerably it
417 did not differ among strains. Finally, mIPSC amplitude was unchanged in *spd*, but
418 significantly greater in the *spa* and *ot* mutants compared to *wt* (35.0 ± 1.9 and 38.5 ±
419 4.0 pA vs 26.5 ± 1.3 pA, respectively). Together, these data suggest $GABA_A$ receptor
420 channel kinetics and release probability in GABAergic terminals on HMs are not
421 altered in any of the mutants. In contrast, and consistent with our recordings from
422 spinal dorsal horn neurons from *spa,* the number of synaptically located $GABA_A$
423 receptors is increased in *spa* and *ot* HMs.

424

425 **Discussion**

426

427 GlyR mutations in the *spasmodic, spastic* and *oscillator* mice result in decreased
428 levels of glycine-mediated inhibitory synaptic transmission and severe motor
429 disturbances (Graham et al. 2006; Simon 1997). Because two of the mutants (*spd* and
430 *spa*) survive to adulthood and reproduce we asked whether the intrinsic and synaptic
431 properties of HMs, which are involved in chewing, swallowing, suckling, vocalization
432 and respiration (Lowe 1980), exhibit homeostatic plasticity in order to maintain
433 network stability in the face of reduced glycinergic drive. We find a number of
434 intrinsic properties, which shape neuronal excitability, are altered in the three mutant
435 strains. The changes were most notable in HMs from the *spa* mouse. The increased
436 GABAergic mIPSC amplitude observed in *spa* and *ot* HMs suggests some sort of
437 synaptic "compensation" has occurred in an attempt to maintain an appropriate level
438 of inhibitory drive that contributes to the survival of *spa* animals but fails in the lethal
439 *ot* mutant. Our major findings are summarized in Figure 7 and suggest, baring the
440 changes we observed in delta-I, that the altered intrinsic and synaptic properties in the
441 *spa* and *ot* mutants are consistent with some form of homeostatic plasticity in
442 response to reduced glycinergic inhibition. In contrast, the increased rebound spiking
443 observed in the *spd* mutant is not consistent with homeostatic plasticity.

444

445 ***Previous work on intrinsic homeostatic plasticity in GlyR mutants***

446 It is now well accepted that 'homeostatic plasticity' prevents hypo- or hyperactivity in
447 neural circuits and that such plasticity can occur via modification of a neuron's
448 intrinsic properties and/or its synaptic inputs (Turrigiano 1999). Biscoe and Duchen
449 (1986) first examined the effect of naturally occurring GlyR mutations in the *spa*
450 mutant. Using an *ex vivo* spinal cord preparation and sharp microelectrode recording
451 they showed RMP, R_{IN}, AHP CURRENT and response to current injection were
452 unaltered in *spa* spinal MNs - even though they concluded *spa* spinal MNs were
453 hyperexcitable based on enhanced responses to dorsal root stimulation. Our data,
454 however, suggest most of the intrinsic properties of *spa* HMs (see next section) are
455 altered in a manner that would make them less responsive to excitatory synaptic
456 inputs (Figure 7). The approaches employed in each study may explain these
457 differences. We studied a different neuron population (HMs vs spinal MNs),
458 employed whole cell patch clamp methods, and activated neurons by current injection

459 versus synaptic stimulation. We, and others, have shown that neurons can respond
460 differently to current injection and synaptic stimulation (Graham et al. 2007a).
461
462 A recent study on the same three GlyR mutants found evidence for intrinsic
463 homeostatic plasticity in medial vestibular nucleus (MVN) neurons (Camp et al.
464 2010). AHP amplitude was increased and this was accompanied by reduced
465 spontaneous firing frequencies and lower gain values (in response to current injection)
466 in MVN neurons from all three mutants. These results differ to our study in three
467 ways. First, the changes in intrinsic properties of HMs differed markedly across the
468 three genotypes. Second, we found no evidence for altered gain in current/frequency
469 plots in HMs (Fig. 3C). Finally, we found the minimum current needed to elicit
470 repetitive discharge (ie, rheobase) shifted to higher values in *spa* mutants. A possible
471 explanation for the differences in intrinsic plasticity observed in MVN neurons is that
472 MVN neurons are spontaneously active, whereas HMs discharge in bursts (Berger
473 2000; Camp et al. 2006; Sekirnjak and du Lac 2002). As HMs are not spontaneously
474 active (Berger 2000), AHP current properties may not be as important in determining
475 neuronal excitability as in MVN neurons.
476
477 ***Differences in intrinsic properties in GlyR mutants***
478 One of the major findings of our study was that the intrinsic properties of HMs differ
479 in the three GlyR mutants. In *spa,* numerous intrinsic properties were altered whereas
480 changes in *spd* and *ot* animals were more limited. Some explanation for the different
481 forms of plasticity lies in the effect of each mutation on GlyRs and inhibitory
482 conductances. For the lethal *ot* mutant the explanation seems straightforward. The
483 only changes in intrinsic properties we observed was a slightly elevated threshold for
484 AP generation and a more negative ΔI (Table 2, Figures 5 and 7): these would reduce
485 and enhance HM excitability, respectively. Whatever the net effect of these changes,
486 even when combined with increased $GABA_A$ergic drive (Table 3, Figures 6B and 7),
487 they are clearly not sufficient to overcome the effects of a complete lack of the adult
488 form ($\alpha 1/\beta$ containing) of the GlyR in the *ot* mutant (Graham et al. 2006; Kling et al.
489 1997).
490

491 In *spd*, the response to hyperpolarizing current injection was the only intrinsic
492 property that differed from *wt* HMs (Fig. 4). Based on sag ratios (Table 2) I_h was
493 similar in the four strains, however, rebound spiking at the offset of the
494 hyperpolarization step was more prevalent in *spd* HMs (Fig. 4B). The increased
495 appearance of rebound spiking in *spd* HMs could be caused by changes in several
496 conductances, including low voltage activated or T-type calcium current, decreased
497 A-current, or altered sodium current expression (Berger 2000). Regardless, they had
498 no affect on RMP, input resistance or the gain of the F/I relationship (Fig. 3) in *spd*
499 HMs. In conclusion, the increased incidence of rebound spiking we observed in *spd*
500 HMs would increase excitability and is therefore not consistent with homeostatic
501 plasticity.
502
503 In contrast to the *ot* and *spd* mutants, HMs in *spa* mice exhibit numerous changes in
504 their intrinsic properties. These include lowered input resistance, increased rheobase
505 current, more depolarized AP threshold, and slower AHP current decay time.
506 Together, these changes would decrease the likelihood of AP discharge during periods
507 of excitatory synaptic input and are consistent with homeostatic plasticity. The more
508 profound intrinsic adaptations in the *spa* versus *spd* mutant may be explained by
509 several observations. First, the *spa* mutation results in a greater reduction in
510 glycinergic drive to HMs. This may activate homeostatic mechanisms to maintain HM
511 output at appropriate levels. We have some evidence for such intrinsic plasticity in
512 dorsal horn neurons. In *spa* neurons the A-type potassium current is increased
513 (Graham et al. 2007b; Graham et al. 2003; Graham et al. 2011). Similarly, we
514 interpreted this as a homeostatic adaptation that would reduce excitability and
515 stabilize dorsal horn circuits in the face of reduced inhibitory drive.
516
517 ***Significance of responses to ramp current injection***
518 Plasticity in persistent inward currents (PICs) is known to be important in both normal
519 and damaged MN circuits. PICs can be revealed in MNs by injecting slow
520 depolarizing and repolarizing current ramps (Bennett et al. 2001b; Hamm et al. 2010;
521 Hounsgaard et al. 1988; Lee and Heckman 1998; Pambo-Pambo et al. 2009; Turkin et
522 al. 2010). They are important for normal motor behaviors in spinal MNs (Heckmann
523 et al. 2005), underlie hyperexcitability associated with spasticity after spinal cord
524 injury (Bennett et al. 2004; ElBasiouny et al. 2010; Gorassini et al. 2004), and

contribute to calcium-mediated excitotoxicity in amyotrophic lateral sclerosis (ElBasiouny et al. 2010; Kuo et al. 2004; Pieri et al. 2009).

There were significant differences in the magnitude of ΔI between *wt* and the *spa* and *ot* mutants (Fig. 5G). In spinal MNs a key indicator of PIC activation is a relatively large and negative ΔI. Surprisingly, ΔI was negative in the *spa* and *ot* mutants and positive in *wt* HMs. This might be interpreted as a modest increase in PIC expression in the *spa* and *ot* mutants. This would lead to increased excitability of *spa* and *ot* HMs: a finding not consistent with homeostatic plasticity. However, the influence of firing rate adaptation also needs to be considered in the overall interpretation of ΔI. Firing rate adaptation, by itself, would tend to produce positive ΔIs and reduce HM excitability (Bennett et al. 2001a; Turkin et al. 2010). Furthermore, the magnitude of firing rate adaptation increases when MNs are driven to discharge at higher frequencies (Kernell 1965; Kernell and Monster 1982). In the present study, all HMs were driven with the ***same*** triangular ramp current. Thus, factors like the more leftward-shifted F/I curve in *wt* versus *spa* and *ot* HMs (Fig. 3C) mean *wt* HMs were driven to fire at higher frequencies during our triangular ramp current stimulus. This could led to greater firing rate adaptation in *wt* HMs, and contribute to their positive ΔI. Future experiments, using ramps that will drive maximal AP firing, are needed to dissect out the effects of firing rate adaptation and PIC enhancement.

GABA compensation in spa and ot mice

The increased GABAergic mIPSC amplitude in the *spa* and *ot* mutants suggests robust GABA compensation occurs in HMs (Figures 6 and 7, Table 3). Surprisingly, GABAergic compensation does not occur in HMs in the *spd* mutant. This result is similar to our previous work on the three mutants in the spinal dorsal horn. In dorsal horn neurons we found that, like the present data on HMs, diminished glycinergic drive was accompanied by a compensatory increase in GABAergic drive in *spa*, but not *spd* (Graham et al. 2003; Graham et al. 2011). In contrast, we found no evidence for GABA compensation in the spinal dorsal horn of *ot* animals despite the increased GABAergic mIPSC amplitude we report here for HMs.

557 For HMs, the differences in the extent of GABA compensation (Figures 6 and 7) in
558 the mutants may be explained by the nature of each mutation. Strychnine binding data
559 suggests GlyR expression in *spd* is similar or only slightly lower than controls in
560 spinal cord homogenates (Graham et al. 2006; Saul et al. 1994). At the receptor level
561 the *spd* mutation reduces glycinergic mIPSC amplitude to ~ 41% of control values
562 (Table 1) and reduces channel open time (Graham et al. 2011; Plested et al. 2007).
563 Together, these factors would significantly reduce total charge transfer during
564 synaptic activation. Thus, it is surprising that GABA compensation does not occur in
565 this mutant. One explanation is that the amplitude of glycinergic inputs, not their time
566 course, is the most important factor in ensuring appropriate glycinergic drive is
567 delivered to the HM motor pool.
568
569 For the *spa* mutation GlyR expression is reduced to 20-30% of controls (Becker 1990;
570 Kling et al. 1997; White and Heller 1982). At the receptor level glycinergic mIPSC
571 amplitude is reduced to ~ 30% of control but channel kinetics are unchanged (Table
572 1). GABA compensation is significant in this mutant (~ 30%, Table 3) and this
573 increased GABAergic drive is consistent with homeostatic plasticity in the face of
574 reduced GlyR function in the *spa* mutant. As noted above, there is evidence for
575 similar homeostatic synaptic plasticity in dorsal horn neurons (Graham et al. 2003).
576 This compensation does not, however, occur in all CNS neurons because there is no
577 evidence of GABA compensation in presumptive spinal MNs in the *spa* animal.
578 Rather, GABAergic drive was decreased, as assessed by the amplitude of evoked
579 IPSCs (von Wegerer et al. 2003). Thus, the interplay between the major inhibitory
580 synaptic transmitter systems (glycine and GABA) is complex and maybe region
581 specific.
582
583 GABA compensation is even greater (~ 40%, Table 3) in *ot* HMs, and is also
584 consistent with homeostatic plasticity in the face of reduced GlyR function. The *ot*
585 mutation is, however, lethal. Perhaps the failure of GABA compensation to "rescue"
586 the mutation is the complete lack of the adult form of the GlyR (ie, $\alpha1/\beta$) in *ot*
587 animals >P14 (Kling et al., 1997). Even though some glycinergic mIPSCs can be
588 recorded in *ot* animals at ~ P19 they are small, have slower kinetics, and are

infrequent (Table 1). In short, the level of glycinergic inhibition they provide is insufficient to support normal motor output in the HM brainstem circuitry.

Conclusions and future directions

Neural networks must maintain stability in the face of constantly changing synaptic inputs, and it is now well established that the nervous system can compensate for changes in synaptic drive to maintain appropriate AP discharge (Nelson and Turrigiano 1998). In the *spd, spa* and *ot* mutants there is a significant reduction in the level of glycinergic inhibitory drive to neurons within the spinal cord and brainstem. This causes severe motor dysfunction in the form of a "startle" syndrome-like phenotype (Simon 1997). We have demonstrated that the intrinsic and synaptic properties of HMs in the *spa* mouse undergo compensatory changes (ie, homeostatic plasticity) that could reduce neuronal excitability to levels required for essential behaviours (like chewing and swallowing). Such homeostatic plasticity was also observed to a lesser extent in the lethal *ot* mutant, in the form of GABA compensation, but this is insufficient to maintain HM excitability at levels compatible with life. Homeostatic plasticity, however, was not observed in the *spd* mouse. This suggests that developmental adaptation to reduced glycinergic inhibition is more complex than just homeostatic plasticity.

610 **References**

611

612 **Barry PH, and Lynch JW**. Liquid junction potentials and small cell effects in patch-
613 clamp analysis. *J Membr Biol* 121: 101-117, 1991.
614 **Bayliss DA, Viana F, Bellingham MC, and Berger AJ**. Characteristics and
615 postnatal development of a hyperpolarization-activated inward current in rat
616 hypoglossal motoneurons in vitro. *J Neurophysiol* 71: 119-128, 1994.
617 **Becker C-M**. Disorders of the inhibitory glycine receptor: the *spastic* mouse. *FASEB*
618 *J* 4: 2767-2774, 1990.
619 **Bennett DJ, Li Y, Harvey PJ, and Gorassini M**. Evidence for plateau potentials in
620 tail motoneurons of awake chronic spinal rats with spasticity. *J Neurophysiol* 86:
621 1972-1982, 2001a.
622 **Bennett DJ, Li Y, and Siu M**. Plateau potentials in sacrocaudal motoneurons of
623 chronic spinal rats, recorded in vitro. *J Neurophysiol* 86: 1955-1971, 2001b.
624 **Bennett DJ, Sanelli L, Cooke CL, Harvey PJ, and Gorassini MA**. Spastic long-
625 lasting reflexes in the awake rat after sacral spinal cord injury. *J Neurophysiol* 91:
626 2247-2258, 2004.
627 **Berger AJ**. Determinants of respiratory motoneuron output. *Respir Physiol* 122: 259-
628 269, 2000.
629 **Berger AJ, Bayliss DA, Bellingham MC, Umemiya M, and Viana F**. Postnatal
630 development of hypoglossal motoneuron intrinsic properties. *Advances in*
631 *Experimental Medicine & Biology* 381: 63-71, 1995.
632 **Biscoe TJ, and Duchen MR**. Synaptic physiology of spinal motoneurones of normal
633 and spastic mice: an in vitro study. *J Physiol* 379: 275-292, 1986.
634 **Buckwalter MS, Cook SA, Davisson MT, White WF, and Camper SA**. A
635 frameshift mutation in the mouse alpha 1 glycine receptor gene (Glra1) results in
636 progressive neurological symptoms and juvenile death. *Hum Mol Genet* 3: 2025-2030,
637 1994.
638 **Button DC, Gardiner K, Marqueste T, and Gardiner PF**. Frequency-current
639 relationships of rat hindlimb alpha-motoneurones. *J Physiol* 573: 663-677, 2006.
640 **Callister RJ, and Graham BA**. Early history of glycine receptor biology in
641 Mammalian spinal cord circuits. *Frontiers in molecular neuroscience* 3: 13, 2010.

642 **Callister RJ, Keast JR, and Sah P**. Ca(2+)-activated K+ channels in rat otic
643 ganglion cells: role of Ca2+ entry via Ca2+ channels and nicotinic receptors. *J*
644 *Physiol* 500 (Pt 3): 571-582, 1997.
645 **Callister RJ, Schofield PR, and Sah P**. Use of murine mutants to study glycine
646 receptor function. *Clin Exp Pharmacol Physiol* 26: 929-931, 1999.
647 **Camp AJ, Callister RJ, and Brichta AM**. Inhibitory synaptic transmission differs in
648 mouse type A and B medial vestibular nucleus neurons, in vitro. *J Neurophysiol* 95:
649 3208-3218, 2006.
650 **Camp AJ, Lim R, Anderson WB, Schofield PR, Callister RJ, and Brichta AM**.
651 Attenuated glycine receptor function reduces excitability of mouse medial vestibular
652 nucleus neurons. *Neurosci* 170: 348-360, 2010.
653 **Cifra A, Nani F, Sharifullina E, and Nistri A**. A repertoire of rhythmic bursting
654 produced by hypoglossal motoneurons in physiological and pathological conditions.
655 *Philos Trans R Soc Lond B Biol Sci* 364: 2493-2500, 2009.
656 **ElBasiouny SM, Schuster JE, and Heckman CJ**. Persistent inward currents in
657 spinal motoneurons: important for normal function but potentially harmful after spinal
658 cord injury and in amyotrophic lateral sclerosis. *Clin Neurophysiol* 121: 1669-1679,
659 2010.
660 **Gorassini MA, Knash ME, Harvey PJ, Bennett DJ, and Yang JF**. Role of
661 motoneurons in the generation of muscle spasms after spinal cord injury. *Brain* 127:
662 2247-2258, 2004.
663 **Graham BA, Brichta AM, and Callister RJ**. Pinch-current injection defines two
664 discharge profiles in mouse superficial dorsal horn neurones, in vitro. *J Physiol* 578:
665 787-798, 2007a.
666 **Graham BA, Brichta AM, Schofield PR, and Callister RJ**. Altered potassium
667 channel function in the superficial dorsal horn of the spastic mouse. *J Physiol* 584:
668 121-136, 2007b.
669 **Graham BA, Schofield PR, Sah P, and Callister RJ**. Altered inhibitory synaptic
670 transmission in superficial dorsal horn neurones in spastic and oscillator mice. *J*
671 *Physiol* 551: 905-916, 2003.
672 **Graham BA, Schofield PR, Sah P, Margrie TW, and Callister RJ**. Distinct
673 physiological mechanisms underlie altered glycinergic synaptic transmission in the
674 murine mutants spastic, spasmodic, and oscillator. *J Neurosci* 26: 4880-4890, 2006.

675 **Graham BA, Tadros MA, Schofield PR, and Callister RJ**. Probing glycine
676 receptor stoichiometry in superficial dorsal horn neurones using the spasmodic
677 mouse. *J Physiol* 589: 2459-2474, 2011.
678 **Hamm TM, Turkin VV, Bandekar NK, O'Neill D, and Jung R**. Persistent currents
679 and discharge patterns in rat hindlimb motoneurons. *J Neurophysiol* 104: 1566-1577,
680 2010.
681 **Heckmann CJ, Gorassini MA, and Bennett DJ**. Persistent inward currents in
682 motoneuron dendrites: implications for motor output. *Muscle Nerve* 31: 135-156,
683 2005.
684 **Hounsgaard J, Hultborn H, Jespersen B, and Kiehn O**. Bistability of alpha-
685 motoneurones in the decerebrate cat and in the acute spinal cat after intravenous 5-
686 hydroxytryptophan. *J Physiol* 405: 345-367, 1988.
687 **Kernell D**. The adaptation and the relation between discharge frequency and current
688 strength of cat lumbosacral motoneurones stimulated by long-lasting injected currents.
689 *Acta Physiol Scand* 65: 65-73, 1965.
690 **Kernell D, and Monster AW**. Time course and properties of late adaptation in spinal
691 motoneurones of the cat. *Exp Brain Res* 46: 191-196, 1982.
692 **Kingsmore SF, Giros B, Suh D, Bieniarz M, Caron MG, and Seldin MF**. Glycine
693 receptor b-subunit gene mutation in *spastic* mouse associated with LINE-1 element
694 insertion. *Nat Genet* 7: 136-142, 1994.
695 **Kling C, Koch M, Saul B, and Becker C-M**. The Frameshift mutation oscillator
696 (Glra1spd-ot) produces a complete loss of glycine receptor alpha1-polypeptide in
697 mouse central nervous system. *Neurosci* 78: 411-417, 1997.
698 **Kuo JJ, Schonewille M, Siddique T, Schults AN, Fu R, Bar PR, Anelli R,**
699 **Heckman CJ, and Kroese AB**. Hyperexcitability of cultured spinal motoneurons
700 from presymptomatic ALS mice. *J Neurophysiol* 91: 571-575, 2004.
701 **Lee RH, and Heckman CJ**. Bistability in spinal motoneurons in vivo: systematic
702 variations in rhythmic firing patterns. *J Neurophysiol* 80: 572-582, 1998.
703 **Legendre P**. The glycinergic inhibitory synapse. *Cell Mol Life Sci* 58: 760-793, 2001.
704 **Lowe AA**. The neural regulation of tongue movements. *Prog Neurobiol* 15: 295-344,
705 1980.
706 **Lynch JW**. Molecular structure and function of the glycine receptor chloride channel.
707 *Physiol Rev* 84: 1051-1095, 2004.

708 **Mody I**. Aspects of the homeostaic plasticity of GABAA receptor-mediated
709 inhibition. *J Physiol (Lond)* 562: 37-46, 2005.
710 **Mülhardt C, Fischer M, Gass P, Simon-Chazottes D, Guénet J-L, Kuhse J, Betz**
711 **H, and Becker C-M**. The spastic mouse: aberrant splicing of glycine receptor b
712 subunit mRNA caused by intronic insertion of L1 element. *Neuron* 13: 1003-1015,
713 1994.
714 **Nelson SB, and Turrigiano GG**. Synaptic depression: a key player in the cortical
715 balancing act. *Nat Neurosci* 1: 539-541, 1998.
716 **Owen AG, and Sherrington CS**. Observations on strychnine reversal. *J Physiol* 43:
717 232-241, 1911.
718 **Pambo-Pambo A, Durand J, and Gueritaud JP**. Early excitability changes in
719 lumbar motoneurons of transgenic SOD1G85R and SOD1G(93A-Low) mice. *J*
720 *Neurophysiol* 102: 3627-3642, 2009.
721 **Pieri M, Carunchio I, Curcio L, Mercuri NB, and Zona C**. Increased persistent
722 sodium current determines cortical hyperexcitability in a genetic model of
723 amyotrophic lateral sclerosis. *Exp Neurol* 215: 368-379, 2009.
724 **Pilarski JQ, Wakefield HE, Fuglevand AJ, Levine RB, and Fregosi RF**.
725 Developmental nicotine exposure alters neurotransmission and excitability in
726 hypoglossal motoneurons. *J Neurophysiol* 105: 423-433, 2011.
727 **Plested AJR, Groot-Kormelink PJ, Colquhoun D, and Sivilotti LG**. Single-
728 channel study of the spasmodic mutation α1A52S in recombinant rat glycine
729 receptors. *J Physiol* 581: 51-73, 2007.
730 **Pratt CA, and Jordan LM**. Ia inhibitory interneurons and Renshaw cells as
731 contributors to the spinal mechanisms of fictive locomotion. *J Neurophysiol* 57: 56-
732 71, 1987.
733 **Rajendra S, and Schofield PR**. Molecular mechanisms of inherited startle
734 syndromes. *Trends Neurosci* 18: 80-82, 1995.
735 **Reali C, Fossat P, Landry M, Russo RE, and Nagy F**. Intrinsic membrane
736 properties of spinal dorsal horn neurones modulate nociceptive information
737 processing in vivo. *J Physiol* 589: 2733-2743, 2011.
738 **Reyes A**. Influence of dendritic conductances on the input-output properties of
739 neurons. *Annu Rev Neurosci* 24: 653-675, 2001.
740 **Ryan SG, Buckwalter MS, Lynch JW, Handford CA, Segura L, Shiang R,**
741 **Wasmuth JJ, Camper SA, Schofield PA, and O'Connell P**. A missense mutation in

742 the gene encoding the a_1 subunit of the inhibitory glycine receptor in the *spasmodic*
743 mouse. *Nat Genet* 7: 131-135, 1994.
744 **Saul B, Schmeiden V, Kling C, Mülhardt C, Gass P, Kuhse J, and Becker C-M**.
745 Point mutation of glycine receptor a1 subunit in the *spasmodic* mouse affects agonist
746 responses. *FEBS Lett* 350: 71-76, 1994.
747 **Sawczuk A, Powers RK, and Binder MD**. Spike frequency adaptation studied in
748 hypoglossal motoneurons of the rat. *J Neurophysiol* 73: 1799-1810, 1995.
749 **Sekirnjak C, and du Lac S**. Intrinsic Firing Dynamics of Vestibular Nucleus
750 Neurons. *J Neurosci* 22: 2083-2095, 2002.
751 **Simon ES**. Involvement of glycine and $GABA_A$ receptors in the pathogenesis of
752 spinal myoclonus: in vitro studies in the isolated neonatal rodent spinal cord.
753 *Neurology* 45: 1883-1892, 1995.
754 **Simon ES**. Phenotypic heterogeneity and disease course in three murine strains with
755 mutations in genes encoding for alpha 1 and beta glycine receptor subunits. *Mov*
756 *Disord* 12: 221-228, 1997.
757 **Singer JH, Talley EM, Bayliss DA, and Berger AJ**. Development of glycinergic
758 synaptic transmission to rat brain stem motoneurons. *J Neurophysiol* 80: 2608-2620,
759 1998.
760 **Takahashi T**. Inward rectification in neonatal rat spinal motoneurones. *J Physiol* 423:
761 47-62, 1990.
762 **Theiss RD, Kuo JJ, and Heckman CJ**. Persistent inward currents in rat ventral horn
763 neurones. *J Physiol* 580: 507-522, 2007.
764 **Turkin VV, O'Neill D, Jung R, Iarkov A, and Hamm TM**. Characteristics and
765 organization of discharge properties in rat hindlimb motoneurons. *J Neurophysiol*
766 104: 1549-1565, 2010.
767 **Turrigiano GG**. Homeostatic plasticity in neuronal networks: the more things
768 change, the more they stay the same. *Trends Neurosci* 22: 221-227, 1999.
769 **Turrigiano GG, Leslie KR, Desai NS, Rutherford LC, and Nelson SB**. Activity-
770 dependent scaling of quantal amplitude in neocortical neurons. *Nature* 391: 892-896,
771 1998.
772 **Turrigiano GG, and Nelson SB**. Homeostatic plasticity in the developing nervous
773 system. *Nat Rev Neurosci* 5: 97-107, 2004.

774 **Umemiya M, and Berger AJ**. Presynaptic inhibition by serotonin of glycinergic
775 inhibitory synaptic currents in the rat brain stem. *J Neurophysiol* 73: 1192-1200,
776 1995.
777 **Viana F, Bayliss DA, and Berger AJ**. Repetitive firing properties of developing rat
778 brainstem motoneurones. *J Physiol* 486: 745-761, 1995.
779 **von Wegerer J, Becker K, Glockenhammer D, Becker CM, Zeilhofer HU, and**
780 **Swandulla D**. Spinal inhibitory synaptic transmission in the glycine receptor mouse
781 mutant spastic. *Neurosci Lett* 345: 45-48, 2003.
782 **White WF, and Heller AH**. Glycine receptor alteration in the mutant mouse *spastic*.
783 *Nature* 298: 655-657, 1982.
784
785
786

787 ***Figure legends***

788 Figure 1. ***Properties of glycinergic mIPSCs in wt and glycine receptor mutant mice.***
789 A. Representative mIPSCs from *wt* and mutant mice. B. Bar plots for group data
790 comparing mIPSC amplitude in the four genotypes. Note, mIPSC amplitude is
791 dramatically reduced in the three mutants (* $p < 0.05$). Data are from Graham et al.,
792 2006.

793

794 Figure 2. ***Comparison of AHP current properties in the four genotypes***. A.
795 Representative AHP current recorded from a *wt* HM in response to a 50 mV voltage
796 step (holding potential -60 mV, 2 ms duration). B. Bar plots comparing mean AHP
797 current amplitude. C. Bar plots comparing the AHP decay time constant. Note, the
798 decay time is longer in the *spa* mutant.

799

800 Figure 3. ***AP discharge in hypoglossal motoneurons during square step current***
801 ***injection.*** A. Representative traces from a *wt* HM in response to increasing levels of
802 current injection (1 s duration). B. Plot of instantaneous frequency versus latency
803 from current step onset for the three different current step responses shown in A.
804 Note, the rapid adaptation that occurs during the first 200 ms of each current step and
805 the relatively constant discharge thereafter. C. Comparison of mean firing frequency
806 versus current step amplitude for the four genotypes. Data have been normalized to
807 rheobase current for each genotype. Note the gains are similar in all four genotypes.

808

809 Figure 4. ***Responses to hyperpolarising current injection.*** A. Left panel shows a trace
810 from a *wt* HM during hyperpolarizing current injection (from - 70 mV, 50 pA
811 increments, 1 s duration). Note the "H-current sag" followed by rebound
812 depolarisation, which in this neuron results in rebound AP discharge. Sag ratio was
813 calculated by comparing membrane potential at the outset (solid arrowhead) and
814 offset (open arrowhead) of the hyperpolarizing current pulse. The right panel shows
815 another type of response in a *wt* HM where the rebound depolarisation does not
816 generate AP discharge. B. Proportions of neurons exhibiting rebound spiking in
817 response to hyperpolarising current compared across genotypes. Significantly more
818 HMs exhibited rebound AP discharge in *spd* versus *wt* neurons (* $p < 0.05$; G-test
819 with Williams' correction).

820

821 Figure 5. ***AP discharge in hypoglossal motoneurons during triangular ramp current***
822 ***injection.*** A. Representative trace from a *wt* HM in response to a 1 nA triangular ramp
823 current, shown in lower panel (black solid line). Delta I (ΔI) was calculated by
824 subtracting the current at which firing ceased (off – dashed line) from the current
825 value where firing commenced (on). A negative ΔI is suggestive of persistent inward
826 currents. B. F/I plot for the HM shown in A. C-D. Frequency histograms for HMs in
827 the four genotypes: ΔI values have been grouped into 25 pA bins. Dark and light bars
828 represent HMs with a negative and positive ΔI values, respectively. G. Plot comparing
829 the *mean* ΔI (pA) for each genotype. The ΔI values in *wt* and *spd* HMs were on
830 average positive, whereas those for *spa* and *ot* were negative and significantly lower
831 than those for *wt* HMs (* $p < 0.05$ different to *wt*, # $p < 0.05$ different to *spd*).
832
833 Figure 6. ***Properties of $GABA_A$ergic mIPSCs in wt and glycine receptor mutant***
834 ***mice.*** A. Representative recordings of $GABA_A$ergic mIPSCs from a *wt* mouse. Top
835 two traces show continuous recordings in the presence of bath applied CNQX (10
836 μM), TTX (1 μM) and strychnine (1 μM). Bottom trace shows the addition of
837 bicuculline (10 μM) blocked all synaptic activity. B. Bar plots for group data
838 comparing $GABA_A$ergic mIPSC amplitude in the four genotypes. Note, mIPSC
839 amplitude is unchanged in *spd* and increased in *spa* and *ot*.(* $p < 0.05$).
840
841 Figure 7. ***Effect of GlyR mutations on synaptic and intrinsic properties of HMs.*** The
842 two photographs illustrate one of the distinguishing phenotypic characteristics of all
843 three GlyR mutants: hindlimb clenching when suspended by the tail. The schematic
844 below compares synaptic and intrinsic properties in HMs for each genotype. In *spd*
845 GlyR mediated synaptic input (red) is reduced and $GABA_AR$ mediated input (orange)
846 is unchanged. Of the intrinsic properties measured only rebound spiking differed from
847 wildtype in the *spd* mutant. This feature would increase HM excitability and is not
848 consistent with homeostatic adaptation. In *spa*, decreased GlyR mediated input is
849 accompanied by increased $GABA_AR$ mediated input and changes in intrinsic
850 properties that combine to reduce HM excitability. Together these changes are
851 consistent with homeostatic adaptation. In *ot*, dramatically decreased GlyR mediated
852 input is accompanied by increased $GABA_AR$ mediated input and minimal adaptation

853 of intrinsic properties. This is consistent with homeostatic adaptation, but is clearly
854 insufficient to maintain appropriate HM output in this lethal mutation.
855

856
857
858 ***Table 1: Properties of glycinergic mIPSCs in wild type and GlyR-mutant HMs.***
859 ***(from Graham et al., 2006)***

Genotype	*Rise time (ms)*	*Amplitude (pA)*	*Decay time (ms)*	*Frequency (Hz)*
Wild Type (*wt*) (n = 23)	0.9 ± 0.1	71.7 ± 3.5	4.9 ± 0.2	1.6 ± 0.3
Spasmodic (*spd*) (n = 20)	0.7 ± 0.1*	29.0 ± 3.0*	2.7 ± 0.2*	1.0 ± 0.3*
Spastic (*spa*) (n = 19)	1.1 ± 0.1	21.0 ± 2.1*	4.6 ± 0.3	0.5 ± 0.1*
Oscillator (*ot*) (n = 15)	1.7 ± 0.1*	19.4 ± 1.8*	12.4 ± 1.2*	0.2 ± 0.1*

860 * differs from *wt*
861
862

863 ***Table 2. Intrinsic properties of wild type and GlyR mutant HMs***

864

	Wild Type (*wt*)	**Spasmodic (*spd*)**	**Spastic (*spa*)**	**Oscillator (*ot*)**
Animal Age (days)	21.3 ± 0.5	25.2 ± 0.8 * (vs. *wt*)	20.3 ± 0.3	18.6 ± 0.1 * (vs. *wt*)
Number of cells	64	48	61	57
Input Resistance (MΩ)	81.3 ± 4.4	75.6 ± 5.1	68.4 ± 3.9 * (vs. *wt*)	75.4 ± 4.1
RMP (mV)	-74.0 ± 0.7	-74.0 ± 1.0	-71.0 ± 1.1 * (vs. *ot*)	-74.5 ± 0.8
AP Threshold (mV)	-55.6 ± 0.5	-55.3 ± 0.7	-51.9 ± 0.7 * (vs. *wt, spd*)	-52.9 ± 0.6* (vs. *wt*)
AP Amplitude (mV)	76.5 ± 1.0	72.8 ± 1.3	68.3 ± 1.5 * (vs. *wt, ot*)	73.8 ± 1.2
AP Half-width (ms)	0.63 ± 0.02	0.67 ± 0.02	0.70 ± 0.03	0.65 ± 0.02
AHP Amplitude (mV)	-27.0 ± 0.6	-27.9 ± 0.9	-26.5 ± 0.9	-29.5 ± 0.8
AHP decay time (ms)	39.0 ± 1.1	40.7 ± 1.8	47.5 ± 2.5* (vs. *wt)*	37.5 ± 1.4
F/I Rheobase (pA)	182 ± 15	176 ± 15	279 ± 25 * (vs. *wt, spd*)	245 ± 23
F/I minimum rate (Hz)	3.9 ± 0.4	4.1 ± 0.4	3.8 ± 0.4	3.8 ± 0.4
F/I gain (Hz/pA)	0.11 ± 0.01	0.08 ± 0.01	0.09 ± 0.01	0.09 ± 0.01
Sag Ratio	1.77 ± 0.04	1.75 ± 0.04	1.77 ± 0.05	1.70 ± 0.04
Rebound Spiking (%)	54.7	75.5* (vs. *wt*)	52.2	48.3
ΔI (pA)	+27.3 ± 10.0	+14.4 ± 9.1	-4.7 ± 8.4 * (vs. *wt*)	-17.7 ± 10.6 * (vs. *wt*)

865 * different to data for the genotype indicated in brackets. AP properties (rows 5-9) are based on APs generated in response to 2 ms step.

866

867
868
869 ***Table 3: Properties of GABAergic mIPSCs in wild type and GlyR-mutant HMs***
870

Genotype	***Rise time (ms)***	***Amplitude (pA)***	***Decay time (ms)***	***Frequency (Hz)***
Wild Type (*wt*) (n = 22)	2.0 ± 0.1	26.5 ± 1.3	14.7 ± 1.0	0.4 ± 0.1
Spasmodic (*spd*) (n = 12)	2.3 ± 0.1	21.1 ± 2.4	16.4 ± 1.9	0.5 ± 0.1
Spastic (*spa*) (n = 13)	2.1 ± 0.2	35.0 ± 1.9*	13.8 ± 0.8	0.7 ± 0.1
Oscillator (*ot*) (n = 11)	2.1 ± 0.1	38.5 ± 4.0*	16.3 ± 1.0	0.5 ± 0.1

871 * differs from *wt*
872
873
874
875
876
877

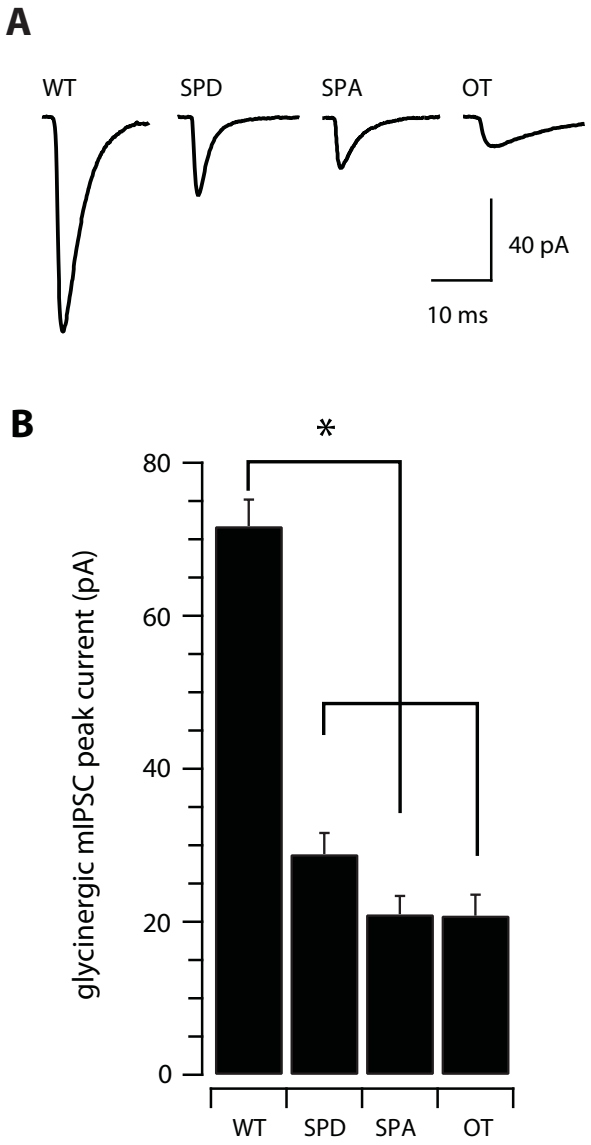

Figure 1. Tadros et al

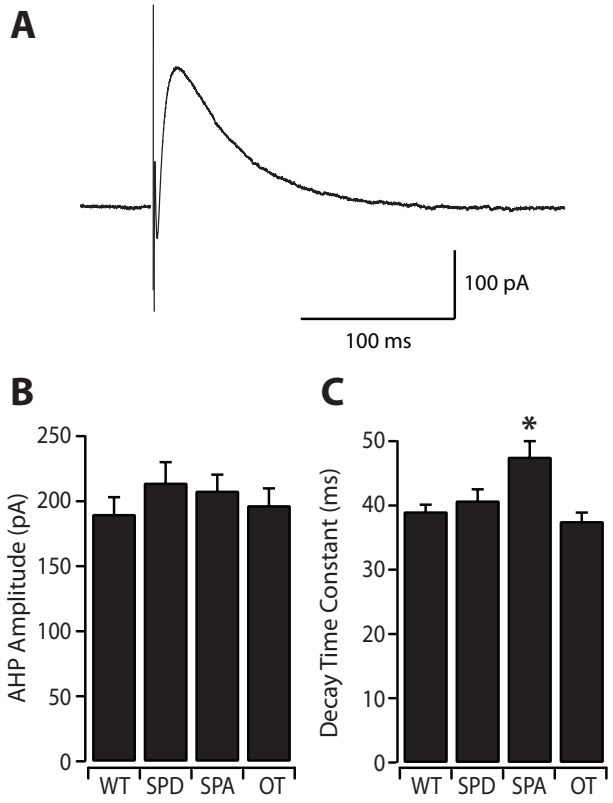

Figure 2. Tadros et al

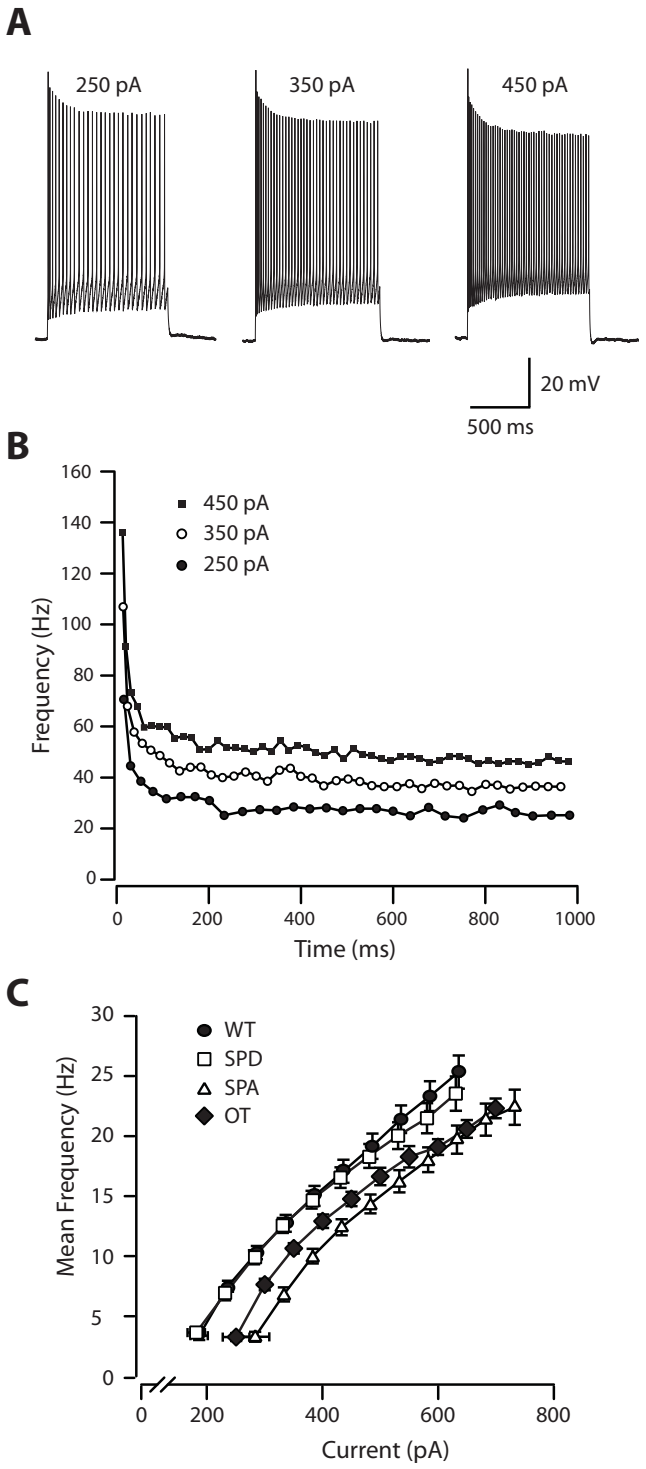

Figure 3. Tadros et al

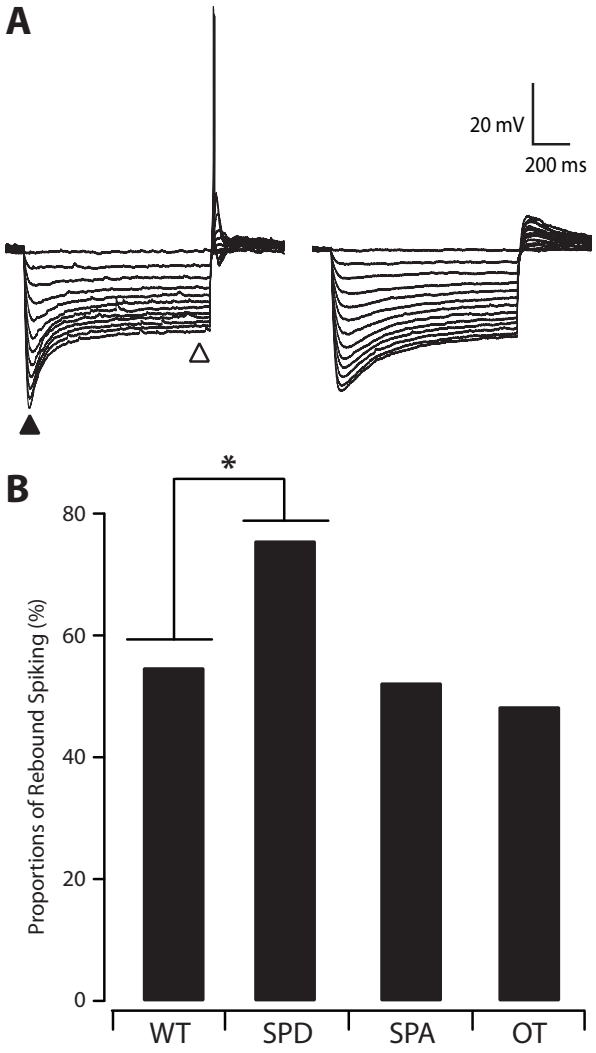

Figure 4. Tadros et al

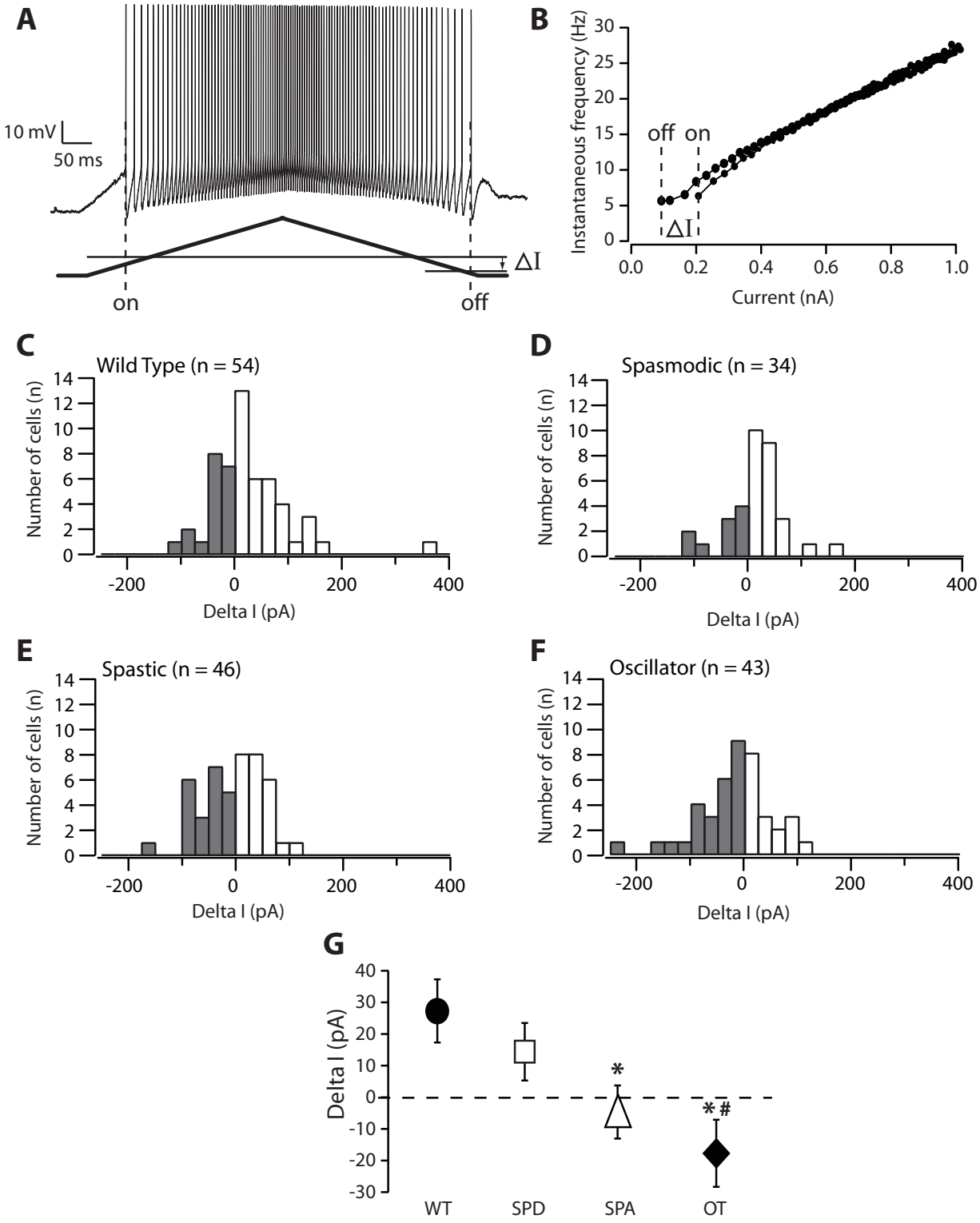

Figure 5. Tadros et al

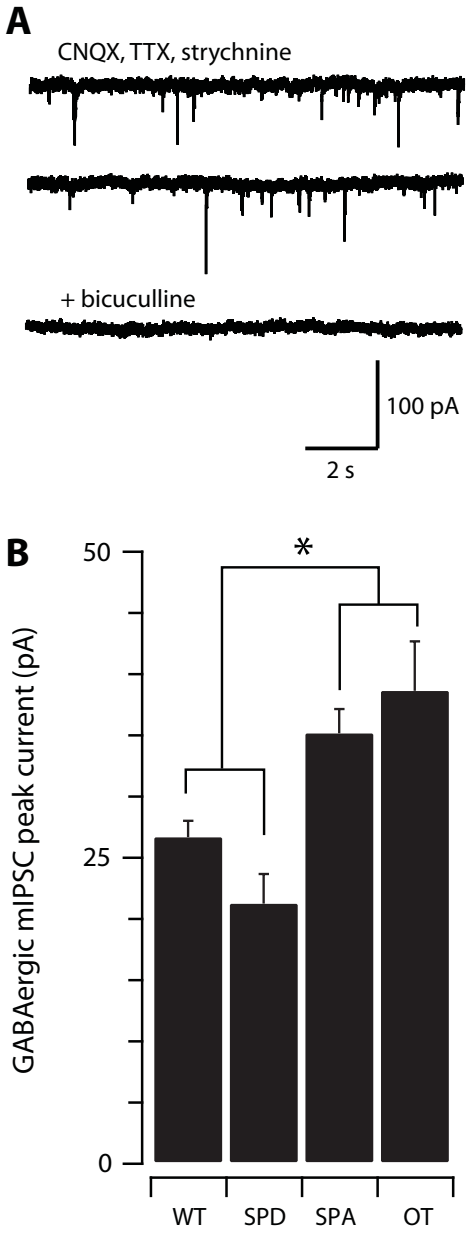

Figure 6. Tadros et al

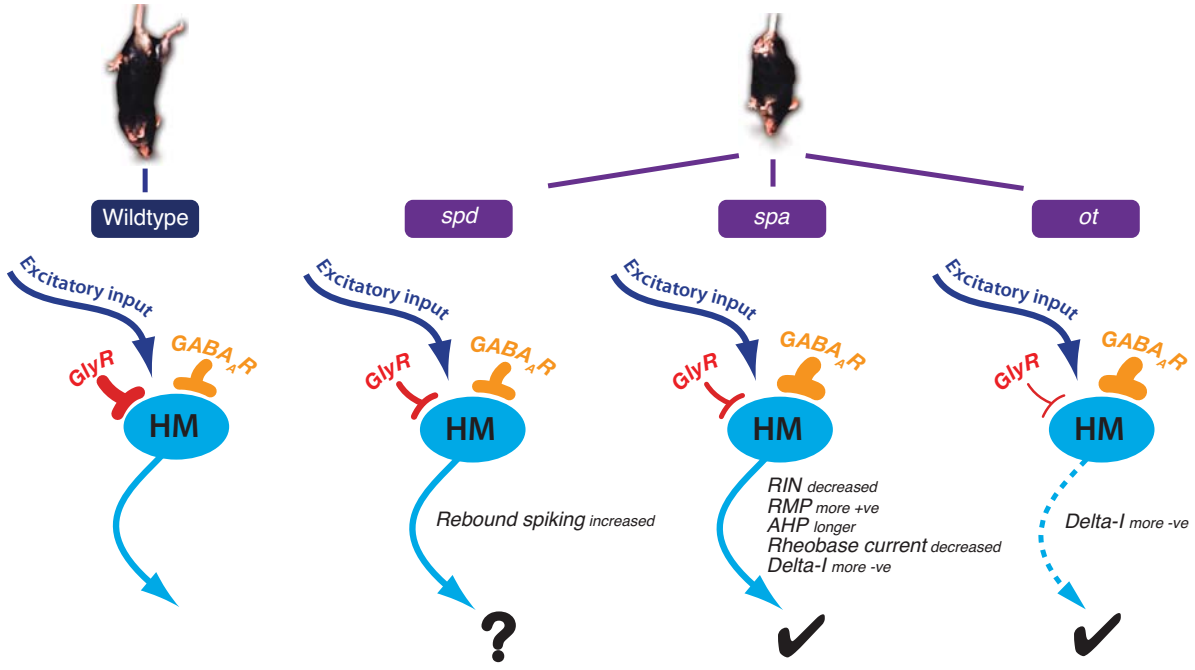

Figure 7. Tadros et al